Terrestrial Gross Primary Production: Using NIR_V to Scale from Site to Globe

Grayson Badgley[1,2,+,*], Leander D.L. Anderegg[1,3,+], Joseph A. Berry[1], Christopher B. Field[2,4]

1. Department of Global Ecology, Carnegie Institution for Science, Stanford, CA, 94305
2. Department of Earth System Science, Stanford University, Stanford, CA, 94305
3. Department of Integrative Biology, University of California, Berkeley, CA, 94720
4. Woods Institute for the Environment, Stanford University, Stanford, CA, 94305

* badgley@stanford.edu

+ These authors contributed equally

Abstract

Terrestrial photosynthesis is the largest and one of the most uncertain fluxes in the global carbon cycle. We find that NIR_V, a remotely sensed measure of canopy structure, accurately predicts photosynthesis at FLUXNET validation sites at monthly to annual timescales ($R^2 = 0.68$), without the need for difficult to acquire information about environmental factors that constrain photosynthesis at short timescales. Scaling the relationship between GPP and NIR_V from FLUXNET eddy covariance sites, we estimate global annual terrestrial photosynthesis to be 147 Pg C y^{-1} (95% credible interval 131-163 Pg C y^{-1}), which falls between bottom-up GPP estimates and the top-down global constraint on GPP from oxygen isotopes. NIR_V-derived estimates of GPP are systematically higher than existing bottom-up estimates, especially throughout the mid-latitudes. Progress in improving estimated GPP from NIR_V can come from improved cloud-screening in satellite data and increased resolution of vegetation characteristics, especially photosynthetic pathway.

Introduction

Terrestrial photosynthesis (or gross primary production (GPP)) is responsible for fixing somewhere between 119 and 169 Pg C y^{-1}, making GPP both the largest and most uncertain component of the global carbon cycle (Anav et al., 2015). Carbon fixed by photosynthesis in turn provides the basis for practically all life on land, providing a strong motivation for improving global estimates of GPP. It is especially important to understand how photosynthesis might respond to global environmental change, as minor perturbations in terrestrial productivity have implications for global biodiversity, agriculture, and climate change (Rockström et al., 2009; Running, 2012).

A global network of eddy covariance measurements of land surface CO_2 exchange serves as the primary basis for quantifying terrestrial photosynthesis at both the site and global scale (Baldocchi et al., 2001; Baldocchi, 2008). Despite their utility, eddy covariance measurements are limited in both time and space; individual flux sites measure CO_2 fluxes over approximately 1 km^2 and, in any given year, fewer than 100 sites operate globally (Kumar et al., 2016). Nevertheless, these sparse measurements are the best available data both for studying ecosystem-scale photosynthetic processes at the global scale and for validating terrestrial ecosystem models, which operate globally at resolutions typically much greater than a single kilometer and need to integrate over processes with time constants from a fraction of a second to many years.

In response to the sparseness of photosynthesis observations, a host of semi-empirical upscaling approaches have emerged for translating site-level CO_2 fluxes to globally gridded photosynthesis estimates. Upscaling depends on the assumption that functional relationships between driver variables and GPP operate the same way at measured and unmeasured sites. Though many upscaling schemes exist, two approaches are by far the most widely used: machine learning (Beer et al., 2010; Tramontana et al., 2016) and remote sensing (Running et al., 2004). Both approaches integrate some combination of site-level abiotic characteristics, plant traits, and meteorology to estimate photosynthesis, using *in situ* fluxes from eddy covariance installations to calculate scaling factors that allow estimation of photosynthesis beyond tower footprints. Such approaches have been quite successful, allowing for both the investigation of the drivers of global photosynthesis (Jung et al., 2017; Zhao et al., 2010) and more extensive benchmarking of photosynthesis models by expanding the temporal and spatial availability of photosynthesis estimates (Bonan et al., 2011; Williams et al., 2009).

Any upscaling introduces uncertainties into GPP estimates, stemming both from model

formulation and input data. Machine learning approaches, for example, provide the best possible constraint on GPP based on available data, but they functionally operate as black boxes. Such complexity makes it difficult to diagnose the causes and consequences of uncertainty. Upscaling approaches are also limited by the availability of and the uncertainties contained within input datasets (e.g., meteorological data). Combined, these challenges limit the utility of existing upscaling approaches for improving our process-based understanding of photosynthesis and determining the true value of global GPP. Of particular concern is the large and persistent disconnect between upscaled estimates of global GPP and higher estimates derived from top-down isotopic constraints (Welp et al., 2011).

Here, we report a novel approach for estimating global GPP using the near-infrared reflectance of vegetation (NIR_V) that takes conceptual root in ideas going back more than 40 years. Even before the widespread use of remote sensing in vegetation analyses, Monteith (1977) observed that the annual increment in biomass growth (net primary production; NPP) can be estimated as the product of the annual absorption of solar radiation and a radiation use efficiency that is relatively constant across species. Several early remote sensing studies built on this idea, documenting the strong correlation between biomass accumulation and the annual integral of the normalized vegetation index (NDVI) (Goward et al., 1985; Tucker et al., 1985). While these approaches for estimating NPP worked well at longer time scales, short-term responses were inconsistent and variable across sites (Running et al., 1988). Progress in improving the performance of NDVI-based productivity models came from a mix of incorporating additional information about vegetation type, meteorology, and physiological stress (Potter et al., 1993; Field et al., 1995; Sellers et al., 1996). As a result, integration approaches gradually transitioned to more physiologically grounded models, which attempt to represent the biochemical processes (e.g., carbon fixation by rubisco) and physiological stress responses (e.g., stomatal closure due to low soil moisture) that control photosynthesis. Though inclusion of biochemical and physiological processes made photosynthesis models more robust at shorter timescales, it introduced the vexing problem of needing to independently specify key physiological parameters, such as the maximum rate of carboxylation of rubisco (V_{Cmax}). Inconsistencies in model parameterization schemes, in turn, give rise to large divergences in model-based estimates of GPP and belie fundamental uncertainties in our understanding of the controls on photosynthesis at the global scale (Schaefer et al., 2012).

We revisit the early strategies for directly relating integrated satellite measurements to plant productivity. Our approach employs the near-infrared reflectance of vegetation (NIR_V), a new

satellite product that approximates the proportion of near-infrared light reflected by vegetation. NIR_V offers several advantages over existing satellite vegetation indices. Namely, NIR_V has a robust physical interpretation, as it relates directly to the number of NIR photons reflected by plants (Badgley et al., 2017). As a result, NIR_V minimizes both the effects soil contamination and variable viewing geometry on satellite-derived spectra. Consequently, NIR_V serves as a comprehensive index of light capture, integrating the influence of leaf area, leaf orientation, and overall canopy structure. We hypothesize that, to the extent plants allocate resources efficiently (Bloom et al., 1985; Field et al., 1995), this integrated measure of investment in light capture should scale with the capacity to fix CO_2, providing a strong basis for new, satellite-derived estimates of GPP.

To test this hypothesis, we use the relationship between NIR_V and *in situ* measurements of GPP derived from eddy covariance. We present our results in three parts. First, we validate the NIR_V-GPP relationship at the site scale, contrasting the NIR_V approach with other remote sensing, statistical, and physiological models of GPP. Second, we extend the relationship to consider global GPP. Third, we evaluate some of the limitations in the global dataset of NIR_V and discuss options for refining the approach.

Materials and Methods

Data

We compared NIR_V, which is the product of the normalized difference vegetation index (NDVI) and NIR reflectance ($NDVI \cdot NIR$), against monthly and annual GPP fluxes at 105 flux sites contained in the FLUXNET2015 Tier 1 dataset that met quality control requirements and fell within the time frame of the MODIS record (2003-present). We calculated median NDVI and NIR for all scenes overlapping a $1km^2$ circle around each fluxsite, using 500 meter, daily red (620-670nm) and near-infrared (NIR, 841-876nm) nadir-adjusted reflectances from MODIS collection MCD43A4.006 hosted on Google Earth Engine for the years spanning 2003 to 2015 (Schaaf et al., 2015). We calculated the average of all NIR_V observations for each month and compared them with monthly estimates of GPP from the FLUXNET2015 dataset (variable name: GPP_VUT_MEAN). We required all site-months to have over 75% valid GPP observations and required site-years to have a minimum of 9 months of data. We gridded the MCD43A4.006 dataset to 0.5° for the global upscaling.

In addition to the site-level comparisons, we evaluated NIR_V-based GPP estimates against two

existing models of GPP: FLUXCOM, a machine learning approach for upscaling FLUXNET observations (Tramontana et al., 2016), and the Breathing Earth System Simulator (BESS), a physiologically based land surface model that has been extensively benchmarked against eddy covariance measurements of GPP (Ryu et al., 2011; Jiang et al., 2016). For FLUXCOM, we used the mean ensemble of annual GPP_HB fluxes from FLUXCOM CRUNCEPv6. For BESS, we used GPP from BESS V1. Site-level RMSE values for FLUXCOM and BESS were derived from data provided by the authors (Tramontana et al., 2016; Jiang et al., 2016). We compared models using an Akaike Information Criterion (AIC) based approach that simultaneously evaluates model accuracy and penalizes model complexity (see Supplementary Text 1 for details). AIC values were calculated for NIR_V, BESS, and FLUXCOM using only site-years shared across all three products.

Calibration

We used Bayesian estimation to relate NIR_V and ecosystem type to GPP at both monthly and annual timescales. Bayesian estimation allowed us to fit slope and intercept, as well as hierarchical variance terms capturing site-level random effects (random deviations from the global slope and intercept per site) and error variance (Gelman et al., 1995). Because Bayesian estimation yields a joint posterior distribution of parameter estimates, upscaling from the model posterior allows us to accurately propagate multiple sources of uncertainty, including joint uncertainty in the model fixed structure (i.e. slope and intercept of the GPP NIR_V relationship) and the random effects (i.e. unexplained site-to-site variation and residual variation in the training dataset). The best model, according to the Deviance Information Criteria (DIC; an AIC-like score modified for Bayesian models), consists of a single, near-zero y-intercept and differing slopes for evergreen, deciduous, and crop ecosystem types. The model includes two additional terms: a random site-level intercept term and an error term, both of which were specified as normal distributions with mean of 0 and variance exponentially related to NIR_V. See Supplementary Text 1 and Table S3 for a full description of the model structure and the Markov chain Monte Carlo fitting procedure, as well as alternative model structures tested. We performed ecosystem type-stratified ten-fold cross-validation at the site level (e.g., leaving out 20% of sites from each ecosystem type) to confirm that the final model was not overfit (Fig. S1).

Upscaling

We produced global annual estimates of GPP using 1000 samples from the joint model posterior for all 0.5° vegetated land pixels from 2005 to 2015. For each posterior sample (i.e. each joint set of scaling and variance parameter estimates), we calculated per-pixel GPP using the scaling parameters for the ecosystem type, a random draw from the site-level error distribution for each pixel and a random draw from the residual error distribution for each pixel-year. Using the site-level model for our global upscaling captured correlations between parameter estimates (scaling slope and site-level variance estimates were often correlated), resulting in GPP estimates that appropriately represent statistical, site, and residual uncertainty from the full joint posterior distribution of the model. We present the median and 95% credible intervals from the distribution of the 1000 global GPP estimates.

Results

Site-level Validation

NIR_V, combined with information on ecosystem type (deciduous, evergreen, and crop) explained 68% of the variation in annual GPP at 105 eddy covariance monitoring sites (526 site-years that passed quality-control and data completeness requirements) and had an RMSE of 0.36 kg C m^{-2} y^{-1} (Fig. 1). At the monthly scale, the same model explained 56% of monthly variation in GPP with an RMSE of 0.08 kg C m^{-2} mo^{-1} (Fig. 1, inset). At the annual scale, we found that the normalized difference vegetation index (NDVI) and the fraction of absorbed photosynthetic radiation (fPAR) (two popular vegetation indices) were worse predictors than NIR_V, explaining 59% and 52% percent of the variation in annual GPP fluxes. The accuracy of NIR_V far exceeded both NDVI and fPAR in terms of RMSE (Table S1). Importantly, the NIR_V-GPP relationship was consistently linear across all values of GPP (Fig. S2). The most parsimonious model included just three ecosystem types, with a single intercept and separate NIR_V-GPP slopes for sites with i) evergreen, ii) deciduous, and iii) crop ecosystem types (Table S2). The model also accounted for variance in both residual error and site-level random intercepts that increased as a function of NIR_V (Fig. S3). Dividing ecosystems into a greater number of types resulted in minor model improvements, but an almost identical DIC with more parameters, causing us to adopt the simpler three ecosystem type model.

The site-level performance of NIR_V-derived GPP compared favorably against BESS and

FLUXCOM, when evaluated across overlapping site-years (Fig. 1B). The RMSE of site-level NIRv-based GPP estimates was 42% lower than estimates from BESS and 57% higher than estimates from FLUXCOM, the machine learning-based upscaling product. However, taking model complexity into account by using the Akaike Information Criterion (AIC) and using conservatively low estimates for number of fitted parameters in the alternative approaches, the NIR_V approach had a far lower AIC than either BESS or FLUXCOM. This indicates that NIR_V better balances model accuracy against model complexity and thereby has a lower likelihood of overfitting the site-level data. Strong performance at validation sites, especially relative to leading statistical and physiological based estimates of GPP, demonstrates that NIR_V provides a robust basis for global estimates of GPP.

Furthermore, the NIR_V approach requires no additional information on meteorological conditions, such as site temperature, vapor pressure deficit, or incoming radiation. Residuals in observed GPP relative to NIR_V-derived GPP estimates showed only weak relationships with meteorological variables (Fig. 2). For site-years with especially high values of annual precipitation, model accuracy was slightly improved by including precipitation in the model. However, including all available meteorological data boosted R^2 by only 0.04, from 0.68 to 0.72 (Table S2), but led to a higher DIC, which indicates that the base NIR_V model better generalizes for predictive purposes. Models combining individual meteorological variables with NIR_V showed similar small improvements in R^2 and RMSE, accompanied by increased DIC (Table S2).

Interestingly, model residuals had only a weak relationship with annual PAR (Fig. 2D, p=0.01, R^2=0.01). Light is the primary driver of photosynthesis at shorter time scales, suggesting that it should be the leading candidate for improving model predictions. This was not the case for estimates based on integrated NIR_V. In fact, including data on integrated PAR decreased the strength of the NIR_V-GPP relationship (Fig. S2D). By requiring fewer inputs, NIR_V-based upscaling of GPP reduces uncertainty from those inputs. It also allows the approach to be applied across a wide range of spatial and temporal scales where such data might not be available.

Global Upscaling

Applying the site-level scaling to globally resolved measurements of NIR_V, we estimated the median value of global annual GPP from 2003 to 2015 to be 147 Pg C y^{-1}, with a 95% credible interval of 131-163 Pg C y^{-1}. This median GPP estimate is intermediate between estimates from bottom-up models and constraints from O_2 isotopes. FLUXCOM places annual GPP at 118 Pg C y^{-1}, while

A

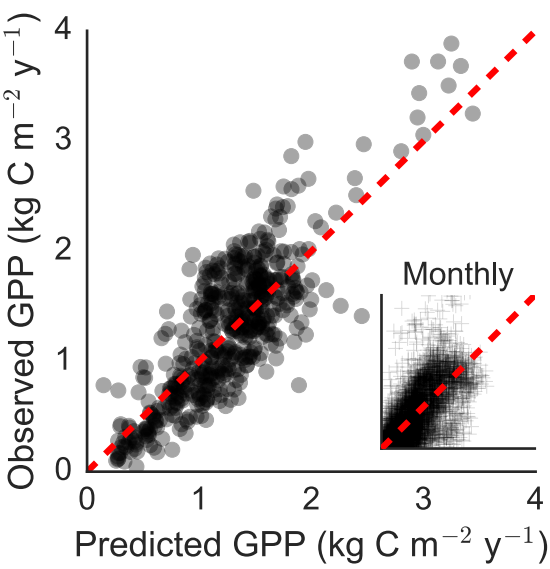

B

GPP Product	RMSE (kg C m^{-2} y^{-1})	AIC
NIR_V	0.36	1736
BESS	0.55	[1837, 1937]
FLUXCOM	0.20	2013

Figure 1. NIR_V explains a substantial portion of site-level GPP at both the monthly and annual timescale. Note the relatively large variation in monthly GPP estimates for low values of observed GPP, as compared to the near-zero intercept in the case of annual fluxes.

BESS puts mean global GPP at 122 Pg C y^{-1}. Based on a meta-analysis, the full range of terrestrial ecosystem models estimate annual to be between 119 and 169 Pg C y^{-1} (Anav et al., 2015). O_2 isotopic measurements are consistent with global annual GPP in the range of 150 to 175 Pg C y^{-1} (Welp et al., 2011).

The spatial distribution of NIR_V-derived GPP is broadly consistent with previous global GPP estimates (Fig. 3). As expected, GPP is concentrated in the tropics and declines toward the poles. On a per biome basis, tropical forests contribute the most , accounting for 31% of global GPP; FLUXCOM and BESS attribute 34% and 33% of GPP to tropical forests, respectively. Though lower in relative terms, NIR_V-derived GPP in tropical forests is 15% higher than both FLUXCOM and BESS GPP estimates. Differences were even larger at higher latitudes, where NIR_V assigns higher productivity to midlatitude mixed forests, grasslands, and shrub-dominated ecosystems (Fig. 3B; Table S3). One recent study that combined solar-induced chlorophyll fluorescence with a terrestrial ecosystem model reports similar relative increases in extratropical GPP (Norton et al., 2018).

On a per pixel basis, NIR_V GPP estimates are strongly linear with GPP estimates from both

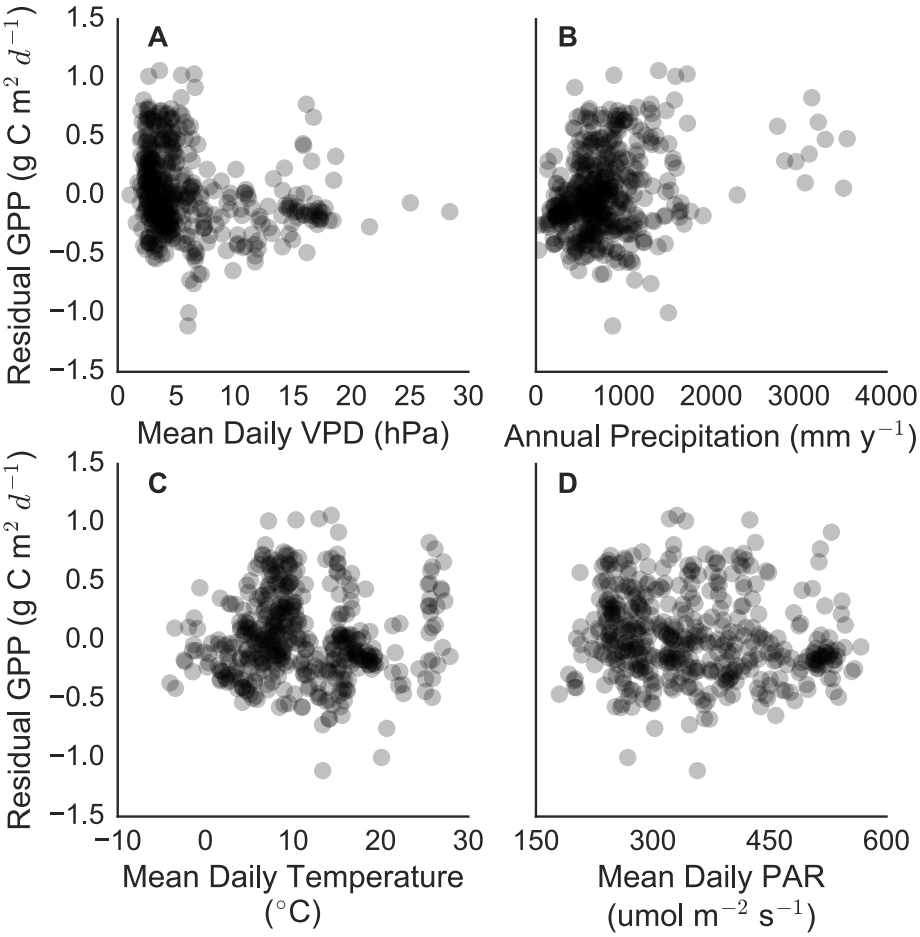

Figure 2. Model residuals of predicted GPP show no strong, systematic variations with site-level meteorological variables. As a result, using meteorological data in conjunction with NIR_V reduces model generality (Table S2). This indicates that NIR_V already captures the dominant influences of climate on canopy development.

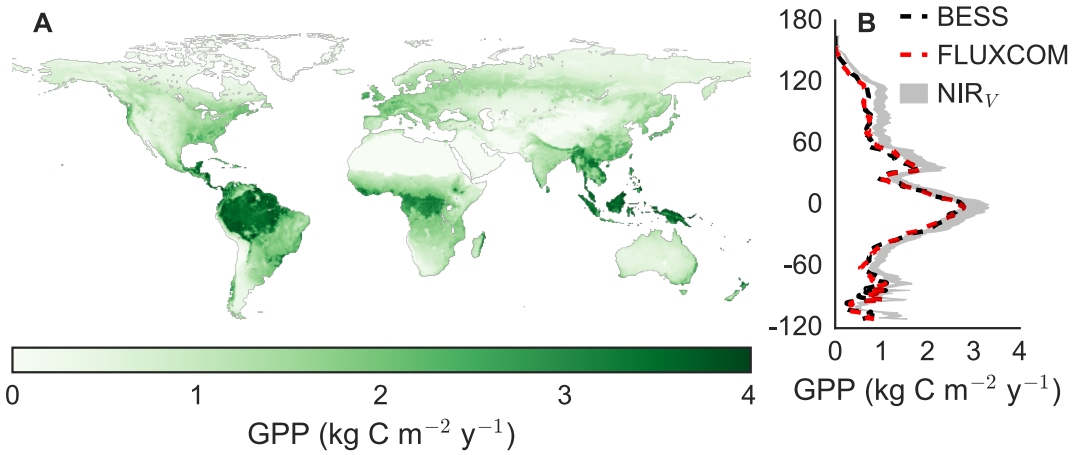

Figure 3. The A) global and B) latitudinal distribution of NIR$_V$-derived GPP. Estimates represent the median of 1000 nearly independent upscalings of NIR$_V$, while the full 95% credible range of GPP is shaded in grey for latitudinal estimates. The latitudinal distribution of annual GPP from FLUXCOM and BESS are shown for comparison.

FLUXCOM and BESS at the annual time scale. R^2 exceeds 0.90 and RMSE is below 0.4 kg C m^{-2} y^{-1} for both products (Fig. S4). This consistency is striking, given that the NIR$_V$ approach requires only two inputs (NIR$_V$ and ecosystem type). By contrast, both FLUXCOM and BESS require numerous environmental inputs. While broadly consistent, the comparison also emphasizes that NIR$_V$-derived GPP estimates are consistently higher, exceeding FLUXCOM GPP by a median value of 0.24 kg C m^{-2} y^{-1} and BESS GPP by 0.21 kg C m^{-2} y^{-1}. There is no obvious reason that NIR$_V$ might be biased high. It might be tempting to think that physiological stress, which is not explicitly accounted for by NIR$_V$, might explain the higher GPP from this approach. However, the NIR$_V$-based approach uses the annual sum of both NIR$_V$ and measured GPP, meaning NIR$_V$-derived GPP estimates are calibrated to include all of the stress effects at FLUXNET sites. The NIR$_V$-based GPP estimates could be biased upwards only if FLUXNET sites are systematically biased toward low-stress locations or the FLUXNET2015 GPP estimates are biased towards good years where stress did not limit photosynthesis. Of course, such biases would affect any upscaling approach calibrated to the FLUXNET2015 dataset. Similarly, using the same satellite data at both the site and global scales minimizes the likelihood that systematic errors or biases in the retrieval of NIR$_V$ affect our estimates of GPP; any error or bias in NIR$_V$ should be accounted for by our site-level calibration. Alternatively, both BESS and FLUXCOM might systematically underestimate true GPP, an interpretation consistent with the constraint from oxygen isotopes (Welp et al., 2011). Resolving this discrepancy represents an important next step in the study photosynthesis at the global scale.

Uncertainty Analysis

Model parsimony, combined with Bayesian estimation, allows us to propagate three sources of uncertainty for each pixel based on the uncertainties quantified in model calibration: statistical (variation in per ecosystem type scaling in the model posterior distribution), site (deviation of each pixel's intercept from the global relationship for that ecosystem type), and residual (otherwise unexplained error). Median per pixel uncertainty is 0.20 kg C m^{-2} y^{-1}. Total uncertainty, comprising all three sources of error, peaks in the tropics where total annual NIR_V is highest. In the worst case, the 95% credible interval of GPP exceeds 0.75 kg C m^{-2} y^{-1} in the Amazon basin and Indonesia (Fig. 4A). Given that tropical forests constitute the highest proportion of GPP (exceeding 30%) and have relatively few flux measurements, high uncertainty throughout the tropics significantly contributes to the overall uncertainty of global GPP estimates, regardless of approach.

Bayesian upscaling allows the uncertainties in parameter estimation from the site-level calibration to be projected globally; two examples of pixel-level uncertainties are shown in Fig. 4B. GPP estimated for each pixel fully contains the uncertainties present in the FLUXNET2015 dataset, providing added confidence in the robustness of credible range of estimated GPP. Outside of pixels with especially low NIR_V, statistical uncertainty is always lowest in both relative and absolute terms, indicating minimal uncertainty in per ecosystem type scaling. On average, site uncertainty is always largest, meaning there is more uncertainty in the NIR_V-GPP relationship from site to site (primarily in the site-level intercept, Fig. S3B) than inter-annual variation (encompassed by residual uncertainty) in the NIR_V-GPP relationship at a single site. Site-to-site variability is randomly distributed, showing no relationship with site climate (Fig. S5), thus highlighting retrieval errors (e.g., soil reflectance, clouds) in NIR_V and inherent uncertainties in eddy covariance derived GPP estimates as the likely cause of site-level uncertainty.

Discussion

NIR_V provides a novel approach for estimating GPP that combines a very simple formulation with excellent performance at validation sites (Fig. 1). As such, the NIR_V approach is largely independent of existing semi-empirical and process-based upscaling approaches. Furthermore, the NIR_V approach achieves strong quantification of uncertainties while maintaining parsimony. This combination of simple calculation plus straightforward analysis and partitioning of uncertainty between model structure and inputs makes NIR_V a useful tool for revisiting and revising

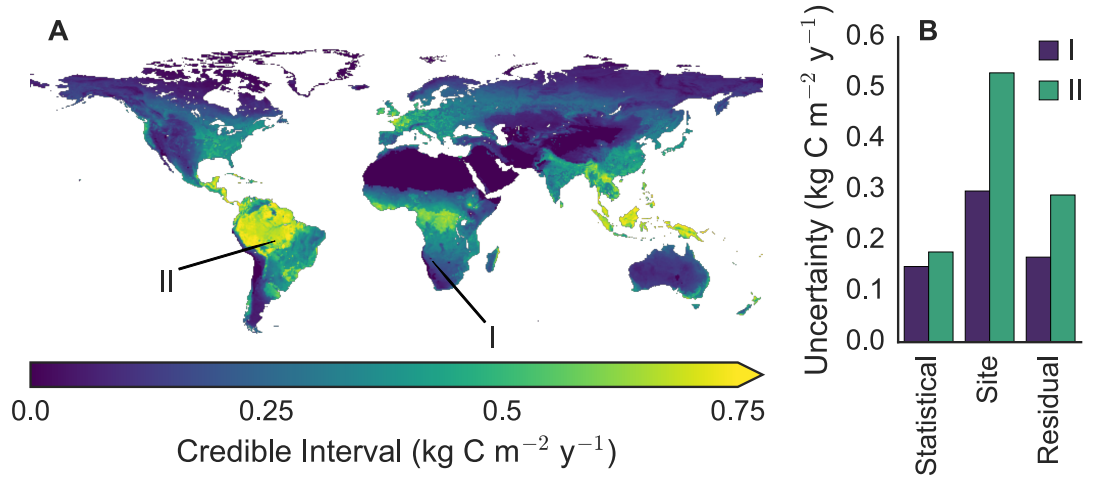

Figure 4. Bayesian hierarchical modeling allows for per pixel error estimation. A) Uncertainty in GPP peaks in the tropics (especially the Amazon and Indonesia), where the credible range of GPP exceed 0.75 kg C m^{-2} y^{-1}. B) Uncertainty can be evaluated on a per pixel basis, where site-level uncertainty is typically largest.

long-standing assumptions about the global controls of photosynthesis.

The strong correlation of NIR_V and GPP at FLUXNET calibration sites provides *prima facie* evidence for the hypothesis that plants allocate resources such that the potential to harvest light (controlled by canopy architecture) and the potential for CO_2 fixation (controlled by physiology and biochemical capacity) are held in balance. To further test this hypothesis, we examined differences in the strength of the NIR_V-GPP relationship at successively longer integration times for evergreen and deciduous validation sites. Relative to evergreens, deciduous leaves have higher photosynthetic rates and must recoup the cost of constructing leaves over a short period of time. Alternatively, evergreen canopies amortize the cost of leaf construction and maintenance over a year or more and, as a result, have less flexibility to respond to short-term perturbations in resource availability (Chabot et al., 1982). Given these contrasting strategies, we expect that NIR_V at deciduous sites should more closely track GPP at short time scales and, as integration time increases from days to months, the performance gap between deciduous and evergreen sites should narrow. This is exactly the pattern found at the FLUXNET validation sites (Fig. 5). At deciduous sites, NIR_V and GPP are highly correlated at even the daily time scale, whereas NIR_V alone is a poor predictor of daily GPP at evergreen sites. By 90 days, the performance of NIR_V as a predictor of GPP is indistinguishable between the two ecosystem types. The coupling of NIR_V and GPP even holds during drought events. During the 2012 North American drought, NIR_V showed characteristic early spring green-up (see Wolf et al., 2016). With the onset of drought at severely drought affected site US-MMS, both NIR_V

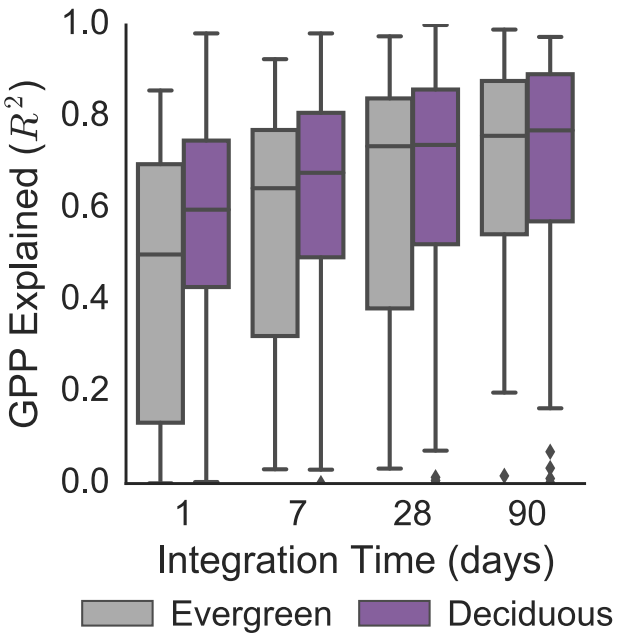

Figure 5. The NIR_V-GPP relationship for deciduous and evergreen canopies at numerous time scales. Deciduous canopies, which require more rapid payback on investments into light capture, exhibit the predicted pattern of more tightly tracking GPP at shorter time scales. Evergreen canopies, which amortize the cost of light capture over multiple years, can afford longer integration times when matching light capture to the availability of other resources.

and GPP rapidly declined in parallel, resulting in a similar NIR_V-GPP relationship as that of non-drought years (Figs. S6A and S6B). Thus, the coupling between the components of canopy structure that influence NIR reflectence and stress-constrained canopy photosynthetic capacity remains strong even at the short timescale of acute stress events. Notably, NDVI showed little deviation compared to non-drought years during the same period (Fig. S6C).

On an instantaneous basis, environmental factors like water, light, and temperature combine with leaf-level biochemical capacity to dictate the rate of photosynthesis (Farquhar et al., 1980). The accuracy of NIR_V for estimating GPP, without the need for additional inputs like total incoming radiation (Fig. 2), does not imply that environmental factors are irrelevant to photosynthesis, but rather that, when integrated over the appropriate time interval, canopy architecture and the physiological controls on photosynthesis are coordinated. This interpretation of the NIR_V-GPP relationship also helps explain why including meteorological data does little to improve the accuracy of NIR_V-derived GPP estimates. If integrated levels of temperature, light, and water availability (as well as nutrients) jointly determine canopy development and physiological potential, then canopy structure, as summarized by NIR_V, should contain the information neccessary to accurately estimate

GPP. The minor improvement from including meteorological data likely indicates that no single linear relationship between one or even multiple meteorological variables accounts for the large number of possible combinations of meteorology and plant response (Fig. 2 and Table S2).

A major strength of the NIR_V approach is that it allows statistically valid error propagation (Fig. 4). More complicated approaches for upscaling GPP make it difficult to accurately partition sources of error, especially model structural errors and errors due to input uncertainties. FLUXCOM, for example, functionally operates as a black box, limiting our ability to draw biological inferences about the global controls of GPP from the model itself. With the NIR_V-based approach, three sources of error warrant consideration. First, it could be the case that even though NIR_V captures many of the controls of GPP, the slowly shifting integrator of NIR_V might contain delays and inconsistencies that introduce uncertainties in the NIR_V-GPP relationship. Second, the coordination of structure and physiology might be imprecise, failing to account for some of the factors that influence GPP. Third, there are almost certainly measurement errors in the NIR_V and GPP datasets used for calibration. The latter two possibilities are strongly suggested by the predominance of site-level error (Fig. 4B and Fig. S3), which indicates that either the physiology controlling the NIR_V-GPP relationship varies from site to site or that the NIR_V and GPP measurements used for calibration lack consistency across space.

A clear illustration of problems with the MODIS data used to calculate NIR_V comes from GF-Guy, an eddy covariance site in French Guyana. GPP fluxes at GF-Guy varied less than 20% month to month, while NIR_V varied by a factor of three (Fig. 6A), which suggests errors in MODIS observations at the site. A likely explanation is cloud contamination, as remote sensing in the tropics is notoriously plagued by clouds. To investigate this, we used the MAIAC data product, newly available for selected sites. MAIAC uses atmospheric modeling to remove aerosols, sub-pixel clouds, and other artifacts from MODIS satellite imagery (Lyapustin et al., 2011). The variability of NIR_V dramatically decreased with the MAIAC data (Fig. 6A). In fact, MAIAC-derived NIR_V had a smaller dynamic range than measured GPP, strongly indicating cloud contamination of the baseline MODIS dataset at GF-Guy and, in all likelihood, throughout the tropics. Cloud contamination in the MODIS data for the tropics likely biases our median global GPP estimate, making 147 Pg C y^{-1} a conservative estimate of global GPP.

Fundamental differences in plant physiology can also contribute to site uncertainty. One clear candidate is the difference in C3 and C4 photosynthesis. C4 plants fix CO_2 more efficiently than C3 plants, which should cause a steeper slope in the NIR_V-GPP relationship, all else equal. Tests at a

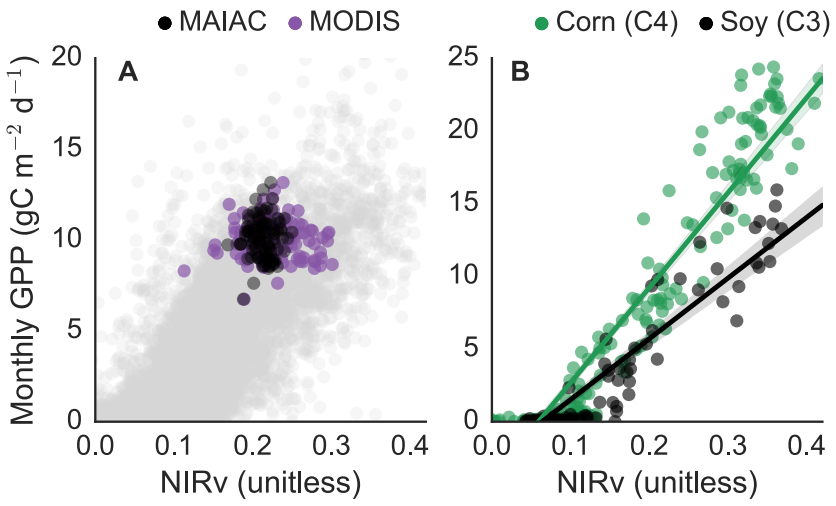

Figure 6. Parsimony allows for the investigation of sources of model uncertainty. A) Cloud contamination drives large monthly variations in MODIS collection 6 NIR_V that are not matched by variations in NIR_V. All monthly data from the FLUXNET2015 dataset shown in grey. B) Photosynthetic pathway predictably alters the NIR_V-GPP relationship, as C4 plants have greater efficiency.

trio of Nebraskan eddy covariance towers that annually rotate between soy (C3) and corn (C4) crops, reveal significant differences in the NIR_V-GPP slope with crop type (Fig. 6B). Including information on the distribution of C3 and C4 vegetation across both wild and managed ecosystems should decrease uncertainty. It would also likely increase the median estimate of GPP, as C3 sites comprise the majority of the calibration dataset, further emphasizing the conservative nature of the 147 Pg C y^{-1} estimate of GPP.

A third advantage of the NIR_V approach is that it can be calculated from existing high-resolution and widely available satellite imagery. This makes NIR_V immediately available for detailed studies and trend analyses at a wide variety of spatial and temporal scales, from individual study sites to the entire globe (Figs. 1 and S3)). Our approach for estimating GPP from NIR_V could also be calculated for the full Landsat and MODIS records, as well as the 39-year record of the Advanced Very High Resolution Radiometer (AVHRR) series of sensors (Tucker et al., 2005). Finally, the ease of measuring NIR_V allows researchers to make inexpensive, canopy-scale spectral measurements that are directly comparable with satellite data, facilitating efforts to bridge spatial scales.

To conclude, NIR_V provides a new, largely independent approach for estimating global GPP with excellent performance at FLUXNET calibration sites. The median estimate from this approach, 147 Pg C y^{-1}, is higher than recent estimate from bottom-up process-based models but is lower than global constraints from oxygen isotopes. Correcting known sources of uncertainty will likely increase

the median estimate. In addition to high accuracy at calibration sites, the approach combines simple calculation, robust error propagation, and the ability to utilize decades of historical remote sensing data. Future refinements of the NIR_V-based approach can come from improved remote sensing inputs and inclusion of additional physiological processes.

Acknowledgments

We thank Jen Johnson and Yoichi Shiga for the many conversations that clarified our thinking, as well as Youngryel Ryu and Mary Whelan, whom reviewed earlier drafts of this work. Gianluca Tramontana and Chongya Jiang kindly provided site-level GPP fluxes for comparison. Bin Peng shared the C3/C4 crop rotation data. Funds from a NASA Earth and Space Science fellowship (G.B.), a NOAA Climate and Global Change fellowship, and NSF Postdoctoral Research Fellowship Grant No. DBI-1711243 (L.D.L.A) supported this research. Any opinions, findings, and conclusions or recommendations expressed in this material are those of the author(s) and do not necessarily reflect the views of the National Science Foundation. This work used eddy covariance data acquired and shared by the FLUXNET community, including these networks: AmeriFlux, AfriFlux, AsiaFlux, CarboAfrica, CarboEuropeIP, CarboItaly, CarboMont, ChinaFlux, Fluxnet-Canada, GreenGrass, ICOS, KoFlux, LBA, NECC, OzFlux-TERN, TCOS-Siberia, and USCCC. The ERA-Interim reanalysis data are provided by ECMWF and processed by LSCE. The FLUXNET eddy covariance data processing and harmonization was carried out by the European Fluxes Database Cluster, AmeriFlux Management Project, and Fluxdata project of FLUXNET, with the support of CDIAC and ICOS Ecosystem Thematic Center, and the OzFlux, ChinaFlux and AsiaFlux offices.

References

Anav, Alessandro, Pierre Friedlingstein, Christian Beer, Philippe Ciais, Anna Harper, Chris Jones, Guillermo Murray-Tortarolo, Dario Papale, Nicholas C Parazoo, Philippe Peylin, et al. (2015). "Spatiotemporal patterns of terrestrial gross primary production: A review". *Reviews of Geophysics* 53.3, pp. 785–818.

Rockström, Johan, Will Steffen, Kevin Noone, Åsa Persson, F Stuart Chapin III, Eric F Lambin, Timothy M Lenton, Marten Scheffer, Carl Folke, Hans Joachim Schellnhuber, et al. (2009). "A safe operating space for humanity". *Nature* 461.7263, pp. 472–475.

Running, Steven W (2012). "A measurable planetary boundary for the biosphere". *Science* 337.6101, pp. 1458–1459.

Baldocchi, Dennis, Eva Falge, Lianhong Gu, Richard Olson, David Hollinger, Steve Running, Peter Anthoni, Ch Bernhofer, Kenneth Davis, Robert Evans, et al. (2001). "FLUXNET: A new tool to study the temporal and spatial variability of ecosystem-scale carbon dioxide, water vapor, and energy flux densities". *Bulletin of the American Meteorological Society* 82.11, pp. 2415–2434.

Baldocchi, Dennis (2008). "'Breathing' of the terrestrial biosphere: lessons learned from a global network of carbon dioxide flux measurement systems". *Australian Journal of Botany* 56.1, pp. 1–26.

Kumar, Jitendra, Forrest M. Hoffman, William W. Hargrove, and Nathan Collier (2016). "Understanding the representativeness of FLUXNET for upscaling carbon flux from eddy covariance measurements". *Earth System Science Data Discussions*.

Beer, Christian, Markus Reichstein, Enrico Tomelleri, Philippe Ciais, Martin Jung, Nuno Carvalhais, Christian Rödenbeck, M Altaf Arain, Dennis Baldocchi, Gordon B Bonan, et al. (2010). "Terrestrial gross carbon dioxide uptake: global distribution and covariation with climate". *Science*, p. 1184984.

Tramontana, Gianluca, Martin Jung, Christopher R Schwalm, Kazuhito Ichii, Gustau Camps-Valls, Botond Ráduly, Markus Reichstein, M Altaf Arain, Alessandro Cescatti, Gerard Kiely, et al. (2016). "Predicting carbon dioxide and energy fluxes across global FLUXNET sites with regression algorithms". *Biogeosciences*.

Running, Steven W, Ramakrishna R Nemani, Faith Ann Heinsch, Maosheng Zhao, Matt Reeves, and Hirofumi Hashimoto (2004). "A continuous satellite-derived measure of global terrestrial primary production". *BioScience* 54.6, pp. 547–560.

Jung, Martin, Markus Reichstein, Christopher R Schwalm, Chris Huntingford, Stephen Sitch, Anders Ahlström, Almut Arneth, Gustau Camps-Valls, Philippe Ciais, Pierre Friedlingstein, et al. (2017). "Compensatory water effects link yearly global land CO 2 sink changes to temperature". *Nature* 541.7638, pp. 516–520.

Zhao, Maosheng and Steven W Running (2010). "Drought-induced reduction in global terrestrial net primary production from 2000 through 2009". *Science* 329.5994, pp. 940–943.

Bonan, Gordon B, Peter J Lawrence, Keith W Oleson, Samuel Levis, Martin Jung, Markus Reichstein, David M Lawrence, and Sean C Swenson (2011). "Improving canopy

processes in the Community Land Model version 4 (CLM4) using global flux fields empirically inferred from FLUXNET data". *Journal of Geophysical Research: Biogeosciences* 116.G2.

Williams, M, AD Richardson, M Reichstein, PC Stoy, P Peylin, Hans Verbeeck, N Carvalhais, M Jung, DY Hollinger, J Kattge, et al. (2009). "Improving land surface models with FLUXNET data". *Biogeosciences* 6.7, pp. 1341–1359.

Welp, Lisa R, Ralph F Keeling, Harro AJ Meijer, Alane F Bollenbacher, Stephen C Piper, Kei Yoshimura, Roger J Francey, Colin E Allison, and Martin Wahlen (2011). "Interannual variability in the oxygen isotopes of atmospheric CO 2 driven by El Niño". *Nature* 477.7366, pp. 579–582.

Monteith, John Lennox (1977). "Climate and the efficiency of crop production in Britain". *Philosophical Transactions of the Royal Society London B* 281.980, pp. 277–294.

Goward, Samuel N, Compton J Tucker, and Dennis G Dye (1985). "North American vegetation patterns observed with the NOAA-7 advanced very high resolution radiometer". *Vegetatio* 64.1, pp. 3–14.

Tucker, Compton J, C Li Vanpraet, MJ Sharman, and Geri Van Ittersum (1985). "Satellite remote sensing of total herbaceous biomass production in the Senegalese Sahel: 1980–1984". *Remote sensing of environment* 17.3, pp. 233–249.

Running, Steven W and Ramakrishna R Nemani (1988). "Relating seasonal patterns of the AVHRR vegetation index to simulated photosynthesis and transpiration of forests in different climates". *Remote Sensing of Environment* 24.2, pp. 347–367.

Potter, Christopher S, James T Randerson, Christopher B Field, Pamela A Matson, Peter M Vitousek, Harold A Mooney, and Steven A Klooster (1993). "Terrestrial ecosystem production: a process model based on global satellite and surface data". *Global Biogeochemical Cycles* 7.4, pp. 811–841.

Field, Christopher B, James T Randerson, and Carolyn M Malmström (1995). "Global net primary production: combining ecology and remote sensing". *Remote sensing of Environment* 51.1, pp. 74–88.

Sellers, PJ, DA Randall, GJ Collatz, JA Berry, CB Field, DA Dazlich, C Zhang, GD Collelo, and L Bounoua (1996). "A revised land surface parameterization (SiB2) for atmospheric GCMs. Part I: Model formulation". *Journal of climate* 9.4, pp. 676–705.

Schaefer, Kevin, Christopher R Schwalm, Chris Williams, M Altaf Arain, Alan Barr, Jing M Chen, Kenneth J Davis, Dimitre Dimitrov, Timothy W Hilton, David Y Hollinger, et al. (2012). "A

model-data comparison of gross primary productivity: Results from the North American Carbon Program site synthesis". *Journal of Geophysical Research: Biogeosciences* 117.G3, G03010.

Badgley, G, C B Field, and J A Berry (2017). "Canopy near-infrared reflectance and terrestrial photosynthesis." *Science Advances* 3.3, e1602244.

Bloom, Arnold J, F Stuart Chapin, and Harold A Mooney (1985). "Resource limitation in plants - an economic analogy". *Annual Review of Ecology and Systematics* 16, pp. 363–392.

Schaaf, C and Z Wang (2015). "MCD43A4 MODIS/Terra+ Aqua BRDF/Albedo Nadir BRDF Adjusted RefDaily L3 Global 500 m V006". *NASA EOSDIS Land Processes DAAC*.

Ryu, Youngryel, Dennis D Baldocchi, Hideki Kobayashi, Catharine van Ingen, Jie Li, T Andy Black, Jason Beringer, Eva Van Gorsel, Alexander Knohl, Beverly E Law, et al. (2011). "Integration of MODIS land and atmosphere products with a coupled-process model to estimate gross primary productivity and evapotranspiration from 1 km to global scales". *Global Biogeochemical Cycles* 25.4.

Jiang, Chongya and Youngryel Ryu (2016). "Multi-scale evaluation of global gross primary productivity and evapotranspiration products derived from Breathing Earth System Simulator (BESS)". *Remote Sensing of Environment* 186, pp. 528–547.

Gelman, Andrew, John B Carlin, Hal S Stern, and Donald B Rubin (1995). *Bayesian data analysis*. Chapman and Hall/CRC.

Norton, A. J., P. J. Rayner, E. N. Koffi, M. Scholze, J. D. Silver, and Y.-P. Wang (2018). "Estimating global gross primary productivity using chlorophyll fluorescence and a data assimilation system with the BETHY-SCOPE model". *Biogeosciences Discussions* 2018, pp. 1–40.

Chabot, Brian F and David J Hicks (1982). "The ecology of leaf life spans". *Annual review of ecology and systematics* 13.1, pp. 229–259.

Wolf, Sebastian, Trevor F Keenan, Joshua B Fisher, Dennis D Baldocchi, Ankur R Desai, Andrew D Richardson, Russell L Scott, Beverly E Law, Marcy E Litvak, Nathaniel A Brunsell, et al. (2016). "Warm spring reduced carbon cycle impact of the 2012 US summer drought". *Proceedings of the National Academy of Sciences* 113.21, pp. 5880–5885.

Farquhar, Graham D, Susan von Caemmerer, and Joseph A Berry (1980). "A biochemical model of photosynthetic CO2 assimilation in leaves of C3 species". *Planta* 149.1, pp. 78–90.

Lyapustin, Alexei, John Martonchik, Yujie Wang, Istvan Laszlo, and Sergey Korkin (2011). "Multiangle implementation of atmospheric correction (MAIAC): 1. Radiative transfer basis and look-up tables". *Journal of Geophysical Research: Atmospheres* 116.D3.

Tucker, Compton J, Jorge E Pinzon, Molly E Brown, Daniel A Slayback, Edwin W Pak, Robert Mahoney, Eric F Vermote, and Nazmi El Saleous (2005). "An extended AVHRR 8-km NDVI dataset compatible with MODIS and SPOT vegetation NDVI data". *International Journal of Remote Sensing* 26.20, pp. 4485–4498.

Supplementary Information for

Terrestrial Gross Primary Production: Using NIR_V to Scale from Site to Globe

Grayson Badgley, Leander D.L. Anderegg, Joseph A. Berry, Christopher B. Field

Grayson Badgley
E-mail: badgley@stanford.edu

This PDF file includes:

Supporting Information Text

Supplementary Text 1: Bayesian Modeling

We used Bayesian estimation to fit linear mixed effects models relating GPP to NIR_V. For the sake of simplicity, we modeled annual or monthly GPP as a linear function of NIR_V, and explored a variety of model structures allowing both slopes and intercepts to differ by land cover class or leaf habit, with random site-level effects. Preliminary model selection suggested that site-level random slope and intercept terms were not needed for the annual model, but were needed for monthly model. For the annual model, we explored a variety of fixed effects structures, as well as a number of variance functions (for residual variation and site-level intercepts). See Table S4 for list of annual models explored and their associated Deviance Information Criteria scores (DIC). All error functions assumed normally distributed errors and similar functional forms for residual error and site random intercepts, but with residual errors being a function of observed annual NIR_V and site random intercepts a function of site mean annual NIR_V. Considerably more complicated model formulations (e.g. estimating retrieval error in NIR_V by treating true NIR_V as a latent variable) are easily implemented in this modeling framework, though we present the simplest defensible case for the sake of illustration and intuitive upscaling. We produced global annual estimates of GPP using the posterior distribution of the best annual NIR_V model (bolded in Table S4). We excluded pixels with a landcover classification of "barren". We have posted the GPP calibration code to www.github.com/badgley/nirv-global.

We used Markov chain Monte Carlo simulations (MCMC) implemented in JAGS to sample the joint posterior distribution of fitted models, with diffuse priors for all parameters (**?**). We ran three parallel MCMC chains, ensuring chain convergence and thinning chains to remove within-chain autocorrelation to produce 1000 nearly independent draws from the posterior. We report median estimates and 95% credible intervals for model parameters, and upscaled GPP estimates, based on the joint posterior distribution of the best model.

Cross Validation

We took the added step of refitting the full Bayesian model using 10-fold cross validation to ensure the robustness of model specification. First, we stratified our data by both site and ecosystem type, assigning 10% of deciduous, evergreen, and crop sites (including all site years for those sites) to each fold. We then fit the model, withholding a single fold, and analyzed the variation of individual model parameters. The mean value of each cross-validated model parameter fell well within the 95% credible interval of the full model posterior distribution for that parameter, indicating the robustness of the full model to changes in training data (Figure S6).

Model Comparison by Modified AIC

We conducted a *post hoc* AIC analysis of BESS, FLUXCOM, and NIR_V-derirved GPP estimates, calculating AIC as: $n \cdot log(MSE) + 2 \cdot p$, where n is the number of site years, MSE is the mean square error of modeled versus observed GPP, and p is the number of fit parameters. We only included site-years in the analysis that were available across all three products. For the comparison products, MSE were calculated using data provided directly from the authors of FLUXCOM and BESS, and number of parameters was estimated extremely conservatively (e.g. assuming only a single parameter per input variable for the FLUXCOM machine learning-base product).

Open Source Software

Python. All analyses, with the exception of the Bayesian modeling, were performed using the Python programming language. We processed netCDF files and tabular data using xarray (1), pandas (2), and numpy (3). We used matplotlib (4) and seaborn (5) for visualization, and Jupyter notebooks for organizing analyses (6).

R. We ran all Bayesian modeling in the R programming environment (7), making use of the "r2jags" package (8) to interface with JAGS, a Bayesian modeling software package (9).

Model	RMSE	Marginal R^2
NIR_V	363.9	0.68
NDVI	410.3	0.59
fPAR	443.4	0.52
$PAR \cdot NIR_V$	454.1	0.50

Table S1. Performance of alternative models, testing the suitability of NDVI, fPAR, and PAR for predicting GPP. NIR_V has the best performance over all metrics.

Model	RMSE	Marginal R2	DIC
NIRv	362.39	0.68	6769.24
NIRv + Precip	350.14	0.70	6774.04
NIRv + Temp	363.23	0.64	6775.41
NIRv + VPD	355.86	0.69	6775.51
NIRv + PAR	360.87	0.68	6773.15
NIRv + All Met	336.77	0.72	6776.86

Table S2. Performance of alternative Bayesian models that include meteorological variables (excluding three site-years without meteorological data). RMSE and R^2 of meteorological models typically outperforms the baseline NIR_V model. However, the NIR_V model has the lowest DIC, indicating the improved performance from including meteorological information comes at the expense of model generality and possible overfitting.

	NIR_V		BESS		FLUXCOM	
	GPP (Pg C y^{-1})	Fraction (%)	GPP (Pg C y^{-1})	Fraction (%)	GPP (Pg C y^{-1})	Fraction (%)
Evergreen Broadleaf forest	46.74	31.70	40.18	33.66	40.48	34.21
Mixed forest	16.28	11.04	10.61	8.89	11.24	9.50
Woody savannas	15.00	10.17	15.21	12.74	14.12	11.94
Savannas	14.79	10.03	13.08	10.96	13.00	10.99
Croplands	13.82	9.38	10.42	8.73	10.48	8.86
Grasslands	12.11	8.21	9.25	7.75	7.84	6.63
Open shrublands	10.89	7.39	6.01	5.04	6.23	5.27
Cropland/Natural vegetation mosaic	9.74	6.61	8.98	7.52	8.64	7.30
Evergreen Needleleaf forest	4.12	2.80	2.69	2.26	2.87	2.42
Other	1.97	1.34	1.69	1.41	1.55	1.31
Deciduous Broadleaf forest	1.96	1.33	1.24	1.04	1.87	1.58

Table S3. Per biome distribution GPP for NIR_V, BESS, and FLUXCOM global GPP products.

Model Structure	Variance Structure	# fixed params	DIC
GPP = intercept + NIR_V:leaf habit	a	4	7142.393
GPP = intercept + NIR_V:leaf habit	$a + b \cdot NIR_V$	4	7134.997
GPP = intercept + NIR_V:leaf habit	$a + e^{zNIR_V \cdot b}$	4	7146.137
GPP = intercept + NIR_V:leaf habit	$a + b \cdot e^{zNIR_V}$	4	7150.204
GPP = intercept + NIR_V:leaf habit	$a + NIR_V^b$	4	7150.299
GPP = intercept + NIR_V:leaf habit	$\boldsymbol{NIR_V^b}$	**4**	**7104.392***
GPP = intercept + NIR_V:leaf habit	$a + b * NIR_V^2$	4	7127.383
GPP = intercept:leaf habit + slope:leaf habit	NIR_V^b	6	7106.333
GPP = intercept:land cover + slope:land cover	NIR_V^b	22	7106.601
GPP = intercept + slope:land cover	NIR_V^b	12	7111.44

Table S4. Potential annual models tested, including various fixed structures and various variance formulations. Variance functions were fit for the standard deviation of both the residual error and the site-level random intercept, where NIR_V is annual observed NIR_V for the residual error and the site mean annual NIR_V for the site random intercept. "$zNIR_V$" indicates that NIR_V values were z-score standardized.

Site	Latitude	Longitude	Years	Reference
AR-Vir	-28.2395	-56.1886	2009–2012	(10)
AT-Neu	47.1167	11.3175	2002–2012	(11)
AU-ASM	-22.283	133.249	2010–2013	(12)
AU-Ade	-13.0769	131.1178	2007–2009	(13)
AU-Cpr	-34.0021	140.5891	2010–2013	(14)
AU-Cum	-33.6133	150.7225	2012–2013	(14)
AU-DaP	-14.0633	131.3181	2008–2013	(13)
AU-DaS	-14.1593	131.3881	2008–2013	(13)
AU-Dry	-15.2588	132.3706	2008–2013	(13)
AU-Emr	-23.8587	148.4746	2011–2013	(15)
AU-Fog	-12.5452	131.3072	2006–2008	(13)
AU-GWW	-30.1913	120.6541	2013–2014	(16)
AU-RDF	-14.5636	132.4776	2011–2013	(13)
AU-Rig	-36.6499	145.5759	2011–2013	(13)
AU-Tum	-35.6566	148.1517	2001–2013	(17)
AU-Whr	-36.6732	145.0294	2011–2013	(14)
BE-Bra	51.3092	4.5206	2000–2013	(18)
BE-Lon	50.5516	4.7461	2004–2014	(19)
BE-Vie	50.3051	5.9981	2000–2014	(20)
BR-Sa3	-3.018	-54.9714	2000–2004	(21)
CA-NS1	55.8792	-98.4839	2002–2005	(22)
CA-NS2	55.9058	-98.5247	2001-2005	(22)
CA-NS3	55.9117	-98.3822	2001–2005	(22)
CA-NS4	55.9117	-98.3822	2002–2005	(22)
CA-NS5	55.8631	-98.485	2001–2005	(22)
CA-NS6	55.9167	-98.9644	2001–2005	(22)
CA-NS7	56.6358	-99.9483	2002–2005	(22)
CA-Qfo	49.6925	-74.3421	2003–2010	(23)
CH-Cha	47.2102	8.4104	2006–2012	(24)
CH-Fru	47.1158	8.5378	2006–2012	(24)
CH-Oe1	47.2858	7.7319	2002–2008	(25)
CN-Cha	42.4025	128.0958	2003–2005	(26)
CN-Cng	44.5934	123.5092	2007–2010	(27)
CN-Dan	30.4978	91.0664	2004–2005	(28)
CN-Din	23.1733	112.5361	2003–2005	(28)
CN-Du2	42.0467	116.2836	2006–2008	(29)
CN-Ha2	37.6086	101.3269	2003–2005	(30)
CN-HaM	37.37	101.18	2002–2004	(31)
CN-Qia	26.7414	115.0581	2003–2005	(28)
CN-Sw2	41.7902	111.8971	2010–2012	(32)
DE-Akm	53.8662	13.6834	2009–2014	http://www.fluxdata.org:8080/sitepages/siteInfo.aspx?DE-Akm
DE-Gri	50.9495	13.5125	2004–2014	(33)
DE-Hai	51.0792	10.453	2000–2012	(34)
DE-Kli	50.8929	13.5225	2004–2014	(35)
DE-Obe	50.7836	13.7196	2008–2014	(36)
DE-RuS	50.8659	6.4472	2011–2014	(37)
DE-Sfn	47.8064	11.3275	2012-2014	(38)
DE-Spw	51.8923	14.0337	2010–2014	http://www.fluxdata.org:8080/sitepages/siteInfo.aspx?DE-spw
DE-Tha	50.9636	13.5669	2000–2014	(39)
DK-Sor	55.4859	11.6446	2000–2012	(40)
ES-LgS	37.0979	-2.9658	2007–2009	(41)
FI-Hyy	61.8475	24.295	2000–2014	(42)
FR-Gri	48.8442	1.9519	2004–2013	(43)
FR-Fon	48.4764	2.7801	2005-2014	(44)
FR-Pue	43.7414	3.5958	2000–2013	(45)
GF-Guy	5.2788	-52.9249	2004–2012	(46)
IT-BCi	40.5238	14.9574	2004-2014	(47)
IT-CA1	42.3804	12.0266	2011–2013	(48)
IT-CA2	42.3772	12.026	2011–2013	(48)

IT-CA3	42.38	12.0222	2011–2013	(48)
IT-Cp2	41.7043	12.3573	2012–2013	(49)
IT-Isp	45.8126	8.6336	2013–2014	(50)
IT-Lav	45.9562	11.2813	2003–2012	(51)
IT-Noe	40.6061	8.1515	2004–2012	(52)
IT-PT1	45.2009	9.061	2002–2004	(53)
IT-Ren	46.5869	11.4337	2000–2013	(54)
IT-Ro1	42.4081	11.93	2000–2008	(55)
IT-Ro2	42.3903	11.9209	2002–2012	(56)
IT-SR2	43.732	10.291	2013–2014	(57)
IT-SRo	43.7279	10.2844	2000–2012	(57)
IT-Tor	45.8444	7.5781	2008–2013	(58)
JP-MBF	44.3869	142.3186	2003–2005	(59)
JP-SMF	35.2617	137.0788	2002–2006	(59)
NL-Hor	52.2404	5.0713	2004–2011	(60)
NL-Loo	52.1666	5.7436	1996–2013	(61)
RU-Fyo	56.4615	32.9221	2000–2013	(62)
SD-Dem	13.2829	30.4783	2005–2009	(63)
US-AR1	36.4267	-99.42	2009–2012	(64)
US-AR2	36.6358	-99.5975	2009–2012	(64)
US-ARM	36.6058	-97.4888	2003–2012	(65)
US-Blo	38.8953	-120.633	2000–2007	(66)
US-Ha1	42.5378	-72.1715	2000–2012	(67)
US-Los	46.0827	-89.9792	2000–2014	(68)
US-MMS	39.3232	-86.4131	2000–2014	(69)
US-Me2	44.4523	-121.5574	2002-2014	(70)
US-Me6	44.3233	-121.608	2010–2012	(71)
US-Myb	38.0498	-121.765	2011–2014	(72)
US-Ne1	41.1651	-96.4766	2001–2013	(73)
US-Ne2	41.1649	-96.4701	2001–2013	(73)
US-Ne3	41.1797	-96.4397	2001–2013	(73)
US-NR1	40.0329	-105.5464	1998-2014	(74)
US-PFa	45.9459	-90.2723	1995-2014	(75)
US-SRG	31.7894	-110.8277	2008-2014	(76)
US-SRM	31.8214	-110.866	2004–2014	(77)
US-Syv	46.242	-89.3477	2001–2014	(78)
US-Ton	38.4316	-120.966	2001–2014	(79)
US-Twt	38.1087	-121.6530	2009-2014	(80)
US-UMB	45.5598	-84.7138	2000-2014	(81)
US-UMd	45.5625	-84.6975	2007–2014	(82)
US-Var	38.4133	-120.951	2000–2014	(83)
US-WCr	45.8059	-90.0799	2000–2014	(84)
US-Whs	31.7438	-110.052	2007–2014	(77)
US-Wkg	31.7365	-109.942	2004–2014	(85)
ZA-Kru	-25.0197	31.4969	2000–2010	(86)
ZM-Mon	-15.4378	23.2528	2007–2009	(87)

Table S5. The FLUXNET2015 sites used in this study.

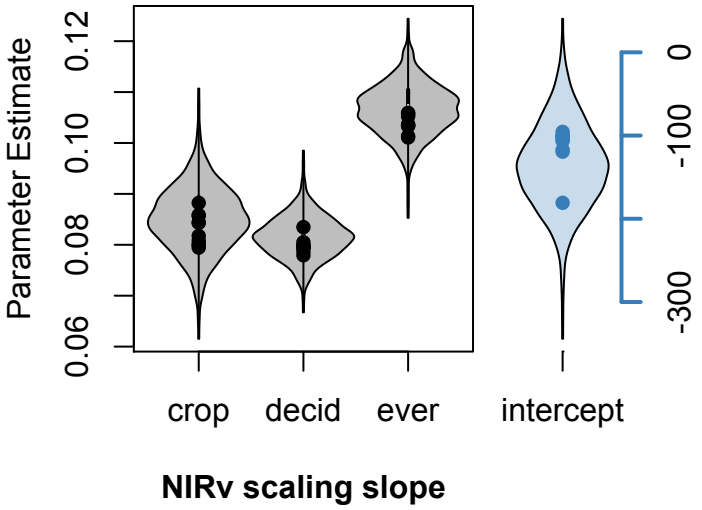

Fig. S1. Comparison of full model posterior parameter estimates versus 10-fold cross validation parameter estimates. Violin plots show the posterior densities for parameter estimates (three scaling slopes and single intercept) from the model trained with all data. Points show the mean parameter estimates for cross validation models after holding each of 10 folds out of model training. Folds were stratified by site and ecosystem-type. All cross validation mean parameter estimates fall within the 95% credible intervals of the full model.

Fig. S2. Predicted GPP values plotted against annual observed GPP at 105 flux sites for A) NIR_V, B) NDVI, C) fPAR, and D) $PAR \cdot NIR_V$.

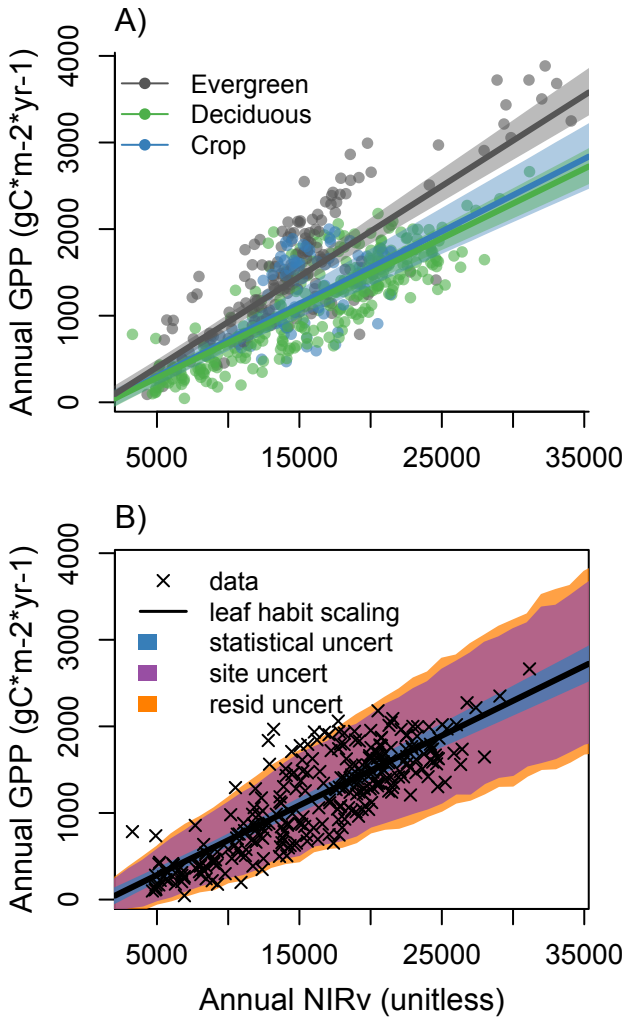

Fig. S3. Depiction of A) the final model formulation and B) the structure of model uncertainties. Each leaf habit shared an intercept, but had slightly different NIR_V to GPP slope. Errors increased exponentially with observed NIR_V, with site-level uncertainty having the largest relative contribution to total per pixel error.

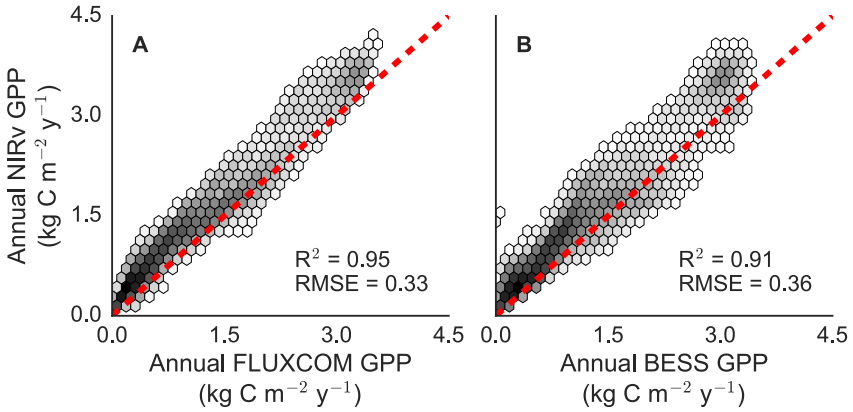

Fig. S4. Upscaled NIR_V-based estimates of annual GPP are linear with both A) FLUXCOM and B) BESS GPP estimates. NIR_V-based estimates tend to be slightly higher than both FLUXCOM and BESS, though NIR_V has low a RMSE relative to both products. NIR_V-based GPP estimate shown as the median case of 1000 nearly independent upscalings, see Methods.

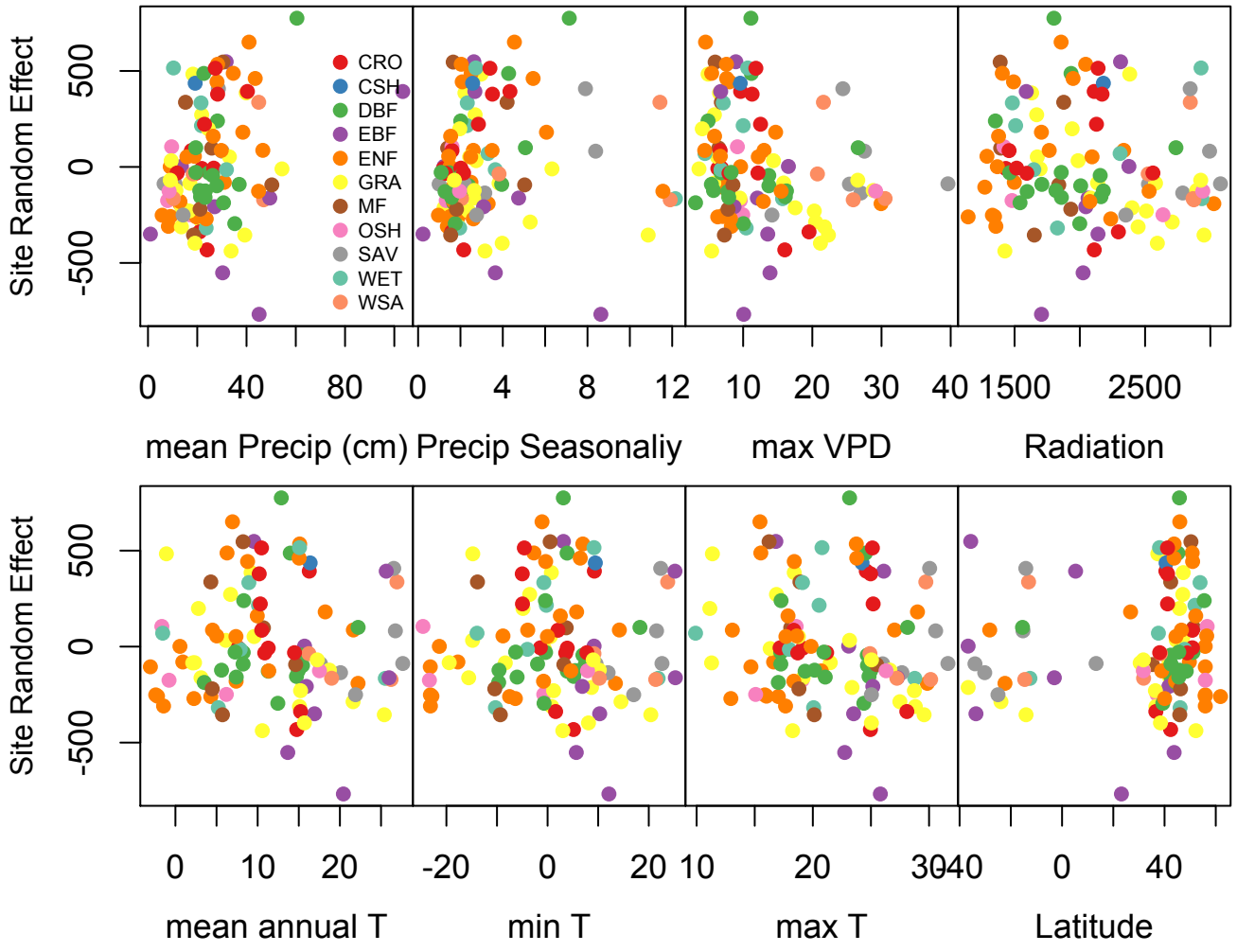

Fig. S5. Site-level random intercepts plotted against various, site-level meteorlogical data show no coherent patterns, indicating that site-to-site uncertainty is a product of uncertainties in NIR_V and GPP used for model calibrations, as opposed to environmental factors not included in the model.

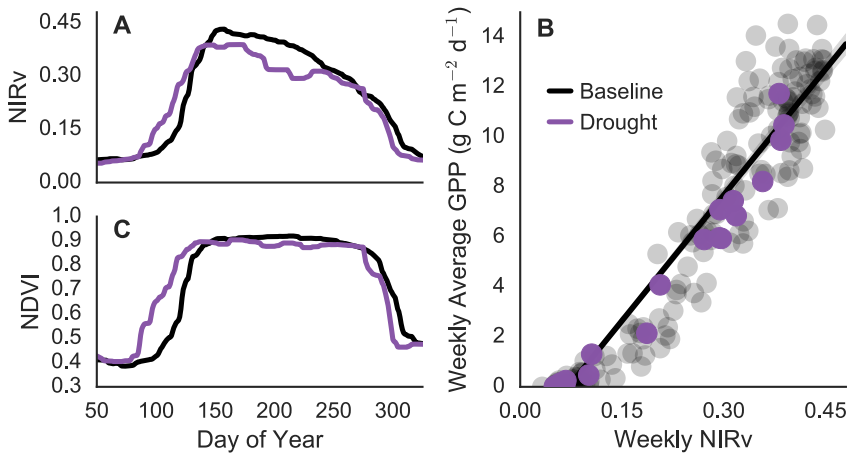

Fig. S6. During the 2012 North American drought, A) NIR_V shows distinctive early spring shift and suppression throughout the summer months when compared against non-drought (baseline) years. B) Despite these phenological changes, NIR_V tightly tracks GPP. C) NDVI during the dourght shows a spring shift, but little difference in peak summer values.

References

1. Hoyer S, Hamman J (2017) xarray: N-D labeled arrays and datasets in Python. *Journal of Open Research Software* 5(1).
2. McKinney W, , et al. (2010) Data structures for statistical computing in python in *Proceedings of the 9th Python in Science Conference*. (Austin, TX), Vol. 445, pp. 51–56.
3. Walt Svd, Colbert SC, Varoquaux G (2011) The numpy array: a structure for efficient numerical computation. *Computing in Science & Engineering* 13(2):22–30.
4. Hunter JD (2007) Matplotlib: A 2d graphics environment. *Computing in science & engineering* 9(3):90–95.
5. Waskom M, et al. (2014) seaborn: v0.5.0 (november 2014).
6. Kluyver T, et al. (2016) Jupyter notebooks – a publishing format for reproducible computational workflows in *Positioning and Power in Academic Publishing: Players, Agents and Agendas*, eds. Loizides F, Schmidt B. (IOS Press), pp. 87 – 90.
7. Team RC (2014) R: A language and environment for statistical computing. r foundation for statistical computing, vienna, austria. 2013.
8. Su YS, Yajima M (2015) R2jags: Using r to run 'jags'. *R package version 0.5-7*.
9. Plummer M (2013) rjags: Bayesian graphical models using mcmc. *R package version* 3(10).
10. Posse G, Lewczuk N, Richter K, Cristiano P (2016) Carbon and water vapor balance in a subtropical pine plantation. *iForest-Biogeosciences and Forestry* 9(5):736.
11. Wohlfahrt G, et al. (2008) Seasonal and inter-annual variability of the net ecosystem co2 exchange of a temperate mountain grassland: Effects of weather and management. *Journal of Geophysical Research: Atmospheres* 113(D8).
12. Eamus D, et al. (2013) Carbon and water fluxes in an arid-zone acacia savanna woodland: An analyses of seasonal patterns and responses to rainfall events. *Agricultural and Forest Meteorology* 182:225–238.
13. Beringer J, Hutley LB, Hacker JM, Neininger B, , et al. (2011) Patterns and processes of carbon, water and energy cycles across northern australian landscapes: From point to region. *Agricultural and Forest Meteorology* 151(11):1409–1416.
14. Karan M, et al. (2016) The australian supersite network: A continental, long-term terrestrial ecosystem observatory. *Science of the Total Environment* 568:1263–1274.
15. Schroder I (2014) Arcturus emerald ozflux tower site. *OzFlux: Australian and New Zealand Flux Research and Monitoring, hdl* 102(100):14249.
16. Prober SM, et al. (2012) Facilitating adaptation of biodiversity to climate change: a conceptual framework applied to the world's largest mediterranean-climate woodland. *Climatic Change* 110(1-2):227–248.
17. Leuning R, Cleugh HA, Zegelin SJ, Hughes D (2005) Carbon and water fluxes over a temperate eucalyptus forest and a tropical wet/dry savanna in australia: measurements and comparison with modis remote sensing estimates. *Agricultural and Forest Meteorology* 129(3-4):151–173.
18. Carrara A, et al. (2003) Net ecosystem co2 exchange of mixed forest in belgium over 5 years. *Agricultural and Forest Meteorology* 119(3-4):209–227.
19. Moureaux C, Debacq A, Bodson B, Heinesch B, Aubinet M (2006) Annual net ecosystem carbon exchange by a sugar beet crop. *Agricultural and Forest Meteorology* 139(1-2):25–39.
20. Aubinet M, et al. (2001) Long term carbon dioxide exchange above a mixed forest in the belgian ardennes. *Agricultural and Forest Meteorology* 108(4):293–315.
21. Miller SD, et al. (2004) Biometric and micrometeorological measurements of tropical forest carbon balance. *Ecological Applications* 14(sp4):114–126.
22. Goulden ML, et al. (2006) An eddy covariance mesonet to measure the effect of forest age on land–atmosphere exchange. *Global Change Biology* 12(11):2146–2162.
23. Bergeron O, et al. (2007) Comparison of carbon dioxide fluxes over three boreal black spruce forests in canada. *Global Change Biology* 13(1):89–107.
24. Eugster W, Zeeman MJ (2006) Micrometeorological techniques to measure ecosystem-scale greenhouse gas fluxes for model validation and improvement in *International Congress Series*. (Elsevier), Vol. 1293, pp. 66–75.
25. Ammann C, Flechard C, Leifeld J, Neftel A, Fuhrer J (2007) The carbon budget of newly established temperate grassland depends on management intensity. *Agriculture, Ecosystems & Environment* 121(1-2):5–20.
26. Zhang JH, Han SJ, Yu GR (2006) Seasonal variation in carbon dioxide exchange over a 200-year-old chinese broad-leaved korean pine mixed forest. *Agricultural and Forest Meteorology* 137(3-4):150–165.
27. Dong G, et al. (2011) Effects of spring drought on carbon sequestration, evapotranspiration and water use efficiency in the songnen meadow steppe in northeast china. *Ecohydrology* 4(2):211–224.
28. Yu GR, et al. (2006) Overview of chinaflux and evaluation of its eddy covariance measurement. *Agricultural and Forest Meteorology* 137(3-4):125–137.
29. Chen S, et al. (2009) Energy balance and partition in inner mongolia steppe ecosystems with different land use types. *Agricultural and Forest Meteorology* 149(11):1800–1809.
30. Fu YL, et al. (2006) Depression of net ecosystem co2 exchange in semi-arid leymus chinensis steppe and alpine shrub. *Agricultural and Forest Meteorology* 137(3-4):234–244.
31. Kato T, et al. (2006) Temperature and biomass influences on interannual changes in co2 exchange in an alpine meadow on the qinghai-tibetan plateau. *Global Change Biology* 12(7):1285–1298.
32. Shao P, Zeng X, Sakaguchi K, Monson RK, Zeng X (2013) Terrestrial carbon cycle: climate relations in eight cmip5 earth system models. *Journal of Climate* 26(22):8744–8764.

33. Gilmanov T, et al. (2007) Partitioning european grassland net ecosystem co2 exchange into gross primary productivity and ecosystem respiration using light response function analysis. *Agriculture, ecosystems & environment* 121(1-2):93–120.
34. Knohl A, Schulze ED, Kolle O, Buchmann N (2003) Large carbon uptake by an unmanaged 250-year-old deciduous forest in central germany. *Agricultural and Forest Meteorology* 118(3-4):151–167.
35. Ceschia E, et al. (2010) Management effects on net ecosystem carbon and ghg budgets at european crop sites. *Agriculture, Ecosystems & Environment* 139(3):363–383.
36. Zimmermann F, Plessow K, Queck R, Bernhofer C, Matschullat J (2006) Atmospheric n-and s-fluxes to a spruce forest—comparison of inferential modelling and the throughfall method. *Atmospheric Environment* 40(25):4782–4796.
37. Mauder M, et al. (2013) A strategy for quality and uncertainty assessment of long-term eddy-covariance measurements. *Agricultural and Forest Meteorology* 169:122–135.
38. Hommeltenberg J, Schmid HP, Drösler M, Werle P (2014) Can a bog drained for forestry be a stronger carbon sink than a natural bog forest? *Biogeosciences* 11(13):3477–3493.
39. GrüNwald T, Bernhofer C (2007) A decade of carbon, water and energy flux measurements of an old spruce forest at the anchor station tharandt. *Tellus B: Chemical and Physical Meteorology* 59(3):387–396.
40. Pilegaard K, Hummelshøj P, Jensen N, Chen Z (2001) Two years of continuous co2 eddy-flux measurements over a danish beech forest. *Agricultural and Forest Meteorology* 107(1):29–41.
41. Reverter BR, et al. (2010) Analyzing the major drivers of nee in a mediterranean alpine shrubland. *Biogeosciences* 7(9):2601–2611.
42. Vesala T, et al. (2005) Effect of thinning on surface fluxes in a boreal forest. *Global Biogeochemical Cycles* 19(2).
43. Loubet B, et al. (2011) Carbon, nitrogen and greenhouse gases budgets over a four years crop rotation in northern france. *Plant and Soil* 343(1-2):109.
44. Delpierre N, Berveiller D, Granda E, Dufrene E (2016) Wood phenology, not carbon input, controls the interannual variability of wood growth in a temperate oak forest. *The New phytologist* 210 2:459–70.
45. Rambal S, Joffre R, Ourcival J, Cavender-Bares J, Rocheteau A (2004) The growth respiration component in eddy co2 flux from a quercus ilex mediterranean forest. *Global Change Biology* 10(9):1460–1469.
46. Bonal D, et al. (2008) Impact of severe dry season on net ecosystem exchange in the neotropical rainforest of french guiana. *Global Change Biology* 14(8):1917–1933.
47. Vitale L, Di Tommasi P, D'Urso G, Magliulo V (2016) The response of ecosystem carbon fluxes to lai and environmental drivers in a maize crop grown in two contrasting seasons. *International Journal of Biometeorology* 60(3):411–420.
48. Sabbatini S, et al. (2016) Greenhouse gas balance of cropland conversion to bioenergy poplar short-rotation coppice. *Biogeosciences* 13(1):95–113.
49. Fares S, Loreto F (2015) Isoprenoid emissions by the mediterranean vegetation in castelporziano. *Rendiconti Lincei* 26(3):493–498.
50. Ferréa C, Zenone T, Comolli R, Seufert G (2012) Estimating heterotrophic and autotrophic soil respiration in a semi-natural forest of lombardy, italy. *Pedobiologia* 55(6):285–294.
51. Cescatti A, ZORER R (2003) Structural acclimation and radiation regime of silver fir (abies alba mill.) shoots along a light gradient. *Plant, Cell & Environment* 26(3):429–442.
52. Spano D, Duce P, Snyder RL, Zara P, Ventura A (2005) Assessment of fuel dryness index on mediterranean vegetation in *Proceedings of the 6th Symposium on Fire and Forest Meteorology, Cammore, Canada.*
53. Migliavacca M, et al. (2009) Seasonal and interannual patterns of carbon and water fluxes of a poplar plantation under peculiar eco-climatic conditions. *Agricultural and Forest Meteorology* 149(9):1460–1476.
54. Marcolla B, et al. (2005) Importance of advection in the atmospheric co2 exchanges of an alpine forest. *Agricultural and Forest Meteorology* 130(3-4):193–206.
55. Rey A, et al. (2002) Annual variation in soil respiration and its components in a coppice oak forest in central italy. *Global Change Biology* 8(9):851–866.
56. Tedeschi V, et al. (2006) Soil respiration in a mediterranean oak forest at different developmental stages after coppicing. *Global Change Biology* 12(1):110–121.
57. Matteucci M, Gruening C, Ballarin IG, Seufert G, Cescatti A (2015) Components, drivers and temporal dynamics of ecosystem respiration in a mediterranean pine forest. *Soil Biology and Biochemistry* 88:224–235.
58. Galvagno M, et al. (2013) Phenology and carbon dioxide source/sink strength of a subalpine grassland in response to an exceptionally short snow season. *Environmental Research Letters* 8(2):025008.
59. Yamazaki T, et al. (2013) A common stomatal parameter set used to simulate the energy and water balance over boreal and temperate forests. *Journal of the Meteorological Society of Japan. Ser. II* 91(3):273–285.
60. Van der Molen M, Gash J, Elbers J (2004) Sonic anemometer (co) sine response and flux measurement: Ii. the effect of introducing an angle of attack dependent calibration. *Agricultural and Forest Meteorology* 122(1-2):95–109.
61. Dolman A, Moors E, Elbers J (2002) The carbon uptake of a mid latitude pine forest growing on sandy soil. *Agricultural and Forest Meteorology* 111(3):157–170.
62. Kurbatova J, Li C, Varlagin A, Xiao X, Vygodskaya N (2008) Modeling carbon dynamics in two adjacent spruce forests with different soil conditions in russia. *Biogeosciences* 5(4):969–980.
63. Sjöström M, et al. (2009) Evaluation of satellite based indices for gross primary production estimates in a sparse savanna in the sudan. *Biogeosciences* 6(1):129–138.

64. Billesbach D, Bradford J (2016) Ameriflux us-ar1 arm usda unl osu woodward switchgrass 1, (AmeriFlux; US Department of Agriculture; University of Nebraska), Technical report.
65. Fischer ML, Billesbach DP, Berry JA, Riley WJ, Torn MS (2007) Spatiotemporal variations in growing season exchanges of co2, h2o, and sensible heat in agricultural fields of the southern great plains. *Earth Interactions* 11(17):1–21.
66. Goldstein A, et al. (2000) Effects of climate variability on the carbon dioxide, water, and sensible heat fluxes above a ponderosa pine plantation in the sierra nevada (ca). *Agricultural and Forest Meteorology* 101(2-3):113–129.
67. Urbanski S, et al. (2007) Factors controlling co2 exchange on timescales from hourly to decadal at harvard forest. *Journal of Geophysical Research: Biogeosciences* 112(G2).
68. Sulman B, Desai A, Cook B, Saliendra N, Mackay D (2009) Contrasting carbon dioxide fluxes between a drying shrub wetland in northern wisconsin, usa, and nearby forests. *Biogeosciences* 6(6):1115–1126.
69. Schmid HP, Grimmond CSB, Cropley F, Offerle B, Su HB (2000) Measurements of co2 and energy fluxes over a mixed hardwood forest in the mid-western united states. *Agricultural and Forest Meteorology* 103(4):357–374.
70. Law BE, et al. (2006) *CARBON FLUXES ACROSS REGIONS: OBSERVATIONAL CONSTRAINTS AT MULTIPLE SCALES*, eds. WU J, JONES KB, LI H, LOUCKS OL. (Springer Netherlands, Dordrecht), pp. 167–190.
71. Ruehr NK, Martin JG, Law BE (2012) Effects of water availability on carbon and water exchange in a young ponderosa pine forest: Above-and belowground responses. *Agricultural and forest meteorology* 164:136–148.
72. Sturtevant C, et al. (2016) Identifying scale-emergent, nonlinear, asynchronous processes of wetland methane exchange. *Journal of Geophysical Research: Biogeosciences* 121(1):188–204.
73. Verma SB, et al. (2005) Annual carbon dioxide exchange in irrigated and rainfed maize-based agroecosystems. *Agricultural and Forest Meteorology* 131(1-2):77–96.
74. Monson RK, et al. (2002) Carbon sequestration in a high-elevation, subalpine forest. *Global Change Biology* 8(5):459–478.
75. Desai AR, et al. (2015) Landscape-level terrestrial methane flux observed from a very tall tower. *Agricultural and Forest Meteorology* 201:61 – 75.
76. Scott RL, Biederman JA, Hamerlynck EP, Barron-Gafford GA (2015) The carbon balance pivot point of southwestern u.s. semiarid ecosystems: Insights from the 21st century drought. *Journal of Geophysical Research: Biogeosciences* 120(12):2612–2624.
77. Scott RL (2010) Using watershed water balance to evaluate the accuracy of eddy covariance evaporation measurements for three semiarid ecosystems. *Agricultural and Forest Meteorology* 150(2):219–225.
78. Desai AR, Bolstad PV, Cook BD, Davis KJ, Carey EV (2005) Comparing net ecosystem exchange of carbon dioxide between an old-growth and mature forest in the upper midwest, usa. *Agricultural and Forest Meteorology* 128(1-2):33–55.
79. Baldocchi DD, Xu L, Kiang N (2004) How plant functional-type, weather, seasonal drought, and soil physical properties alter water and energy fluxes of an oak–grass savanna and an annual grassland. *Agricultural and Forest Meteorology* 123(1-2):13–39.
80. Hatala JA, et al. (2012) Greenhouse gas (co2, ch4, h2o) fluxes from drained and flooded agricultural peatlands in the sacramento-san joaquin delta. *Agriculture, Ecosystems Environment* 150:1 – 18.
81. Rothstein DE, Zak DR, Pregitzer KS, Curtis PS (2000) Kinetics of nitrogen uptake by populus tremuloides in relation to atmospheric co2 and soil nitrogen availability. *Tree Physiology* 20(4):265–270.
82. Gough CM, et al. (2013) Sustained carbon uptake and storage following moderate disturbance in a great lakes forest. *Ecological Applications* 23(5):1202–1215.
83. Ma S, Baldocchi DD, Xu L, Hehn T (2007) Inter-annual variability in carbon dioxide exchange of an oak/grass savanna and open grassland in california. *Agricultural and Forest Meteorology* 147(3-4):157–171.
84. Cook BD, et al. (2004) Carbon exchange and venting anomalies in an upland deciduous forest in northern wisconsin, usa. *Agricultural and Forest Meteorology* 126(3-4):271–295.
85. Scott R (2016) Ameriflux us-wkg walnut gulch kendall grasslands, (AmeriFlux; United States Department of Agriculture), Technical report.
86. Scholes R, et al. (2001) The environment and vegetation of the flux measurement site near skukuza. *Koedoe* pp. 73–83.
87. Scanlon T, Albertson J (2004) Canopy scale measurements of co2 and water vapor exchange along a precipitation gradient in southern africa. *Global Change Biology* 10(3):329–341.